



# Numerical simulation of non-linear heat conduction subjected to a laser source: the effects of variable thermal properties

Gustavo Gutierrez, Tien-Chen Jen\*

*Mechanical Engineering Department, University of Wisconsin, Milwaukee, WI 53211, USA*

Received 26 March 1999; received in revised form 3 September 1999

## Abstract

This paper presents a numerical study of the temperature distribution in a body subjected to a spatially exponential decaying laser source. The governing heat conduction equation, the boundary conditions and the initial condition are presented in a dimensionless form as a function of a group of dimensionless parameters, namely,  $\chi$ ,  $\tau$ ,  $Bi$ ,  $w$ ,  $c_1$ ,  $c_2$  and  $c_3$ . Three different sets of thermal boundary conditions imposed at the “far” boundary, including convection, insulated and constant surface temperature conditions are investigated in the present study. The governing equation is discretized using a control volume approach, with a variable grid to increase the resolution of the domain near the boundary where the laser heat source is applied. The effects of the different parameters and the temperature dependent thermal properties are studied in detail. The calculated results are compared with previous analytical studies for constant thermal properties obtained for both semi-infinite and finite domains. Finally, the present numerical solutions are compared to existing experimental data. © 2000 Elsevier Science Ltd. All rights reserved.

*Keywords:* Conduction; Laser materials processing; Variable thermal properties

## 1. Introduction

The use of lasers in material processing has gained significant attention in the past decade. In non-reactive processes, the laser beam is used to modify the target material structure by local heating. This local heating alters the material crystalline structure and thus, the electrical, mechanical and thermal properties. For reliability and consistency, it

is necessary to be able to control effectively the induced structural changes. It is therefore important to understand and quantify the effects of thermal transport in the film structures. In particular, the use of laser in machining operations has been studied theoretically and experimentally [1,2,9,14,15,17,18,20]. An important mechanism, called “explosive removal of material”, was observed by Dabby and Paek [2]. This phenomenon occurs when a highly localized laser energy beam paints the exposed surface. A plausible explanation given by Blackwell [1] was that before phase change occurs at the surface, the location of the maximum temperature moves inside the workpiece due to con-

\* Corresponding author. Tel.: +1-414-229-2307; fax: +1-414-229-6958.

*E-mail address:* jen@cae.uwm.edu (T.-C. Jen).

**Nomenclature**

$B$	dimensionless laser source constant	$\{b_{\text{inf}}\}$	vector associated with convection boundary conditions
$Bi$	Biot number	$[I]$	identity matrix
$c_1$	dimensionless coefficient for the reduced thermal conductivity $\kappa$	$[K]$	matrix of coefficients
$c_2$	dimensionless coefficient for the reduced heat capacity $\gamma$	$\{Q\}$	vector of heat source
$c_3$	dimensionless coefficient for the reduced heat capacity $\gamma$	<i>Greek symbols</i>	
$C_p$	heat capacity	$\alpha$	thermal diffusivity ( $\alpha = k_0/\rho C_{p0}$ )
$I_0$	reference laser irradiation	$\beta$	laser source constant
$h$	convective heat transfer coefficient	$\eta$	weighted factor for time integration
$k$	thermal conductivity	$\mu$	absorption coefficient
$k_1$	coefficient for the thermal conductivity $k$	$\rho$	density
$k_2$	coefficient for the heat capacity $C_p$	$\theta$	temperature rise above the initial temperature
$k_3$	coefficient for the heat capacity $C_p$	$\tau$	dimensionless time (Fourier number)
$L$	length of the body	$\Delta$	increment
$\chi^*$	dimensionless length of the body	$\chi$	transformed spatial coordinate
$nx$	maximum number of nodes	$\chi_\xi$	metric of the transformation
$q'''$	heat source	$\xi$	spatial coordinate
$q^*$	dimensionless heat source	<i>Subscripts</i>	
$R$	surface reflectance	$E, W, P$	values of the variable at nodes $E, W$ and $P$ , respectively
$T$	temperature	$EP$	average value of the variable between nodes $E$ and $P$
$T_0$	ambient temperature	$WP$	average value of the variable between nodes $W$ and $P$
$T_\infty$	free stream temperature	1	value of the property at node 1
$t$	time	$nx$	value of the property at node $nx$
$u$	dimensionless temperature	<i>Superscripts</i>	
$x$	spatial variable	$n$	value of the variable at time $n$
$w$	dimensionless energy absorption at surface	$n + 1$	value of the variable at time $n + 1$
$[A]$	matrix equal to $I - \eta K \Delta \tau$		
$[B]$	matrix equal to $I - (1 - \eta) K \Delta \tau$		
$\{b_n\}$	vector equal to $[B]\{u\}^n$		
$\{b_c\}$	vector associated with Dirichlet boundary conditions		

vective and radiative heat losses from the surface to the surrounding. Thus, the material under the surface will melt first. If the material expands during the phase change, explosive material removal could occur. Blackwell [1] showed that the location of the maximum temperature moves inside the workpiece when the Biot number is greater than 0.05 (i.e., when there is efficient cooling at the surface due to convection). Very recently, Zubair and Chaudhry [20] discussed the fundamental problem considered by Blackwell [1], and revisited the problem to include the general time-dependent laser heat source. Yilbas and Sami [19] found an analytical solution for the case where a time-dependent laser heat source is applied to a semi-infinite body with insulated exposed surface boundary condition.

It should be noted that all previously published

studies are for the semi-infinite geometry. This is a good assumption only when the heat penetration depth is much smaller than the thickness of the body. When the body under consideration is very thin or the laser heating time is relatively large, the heat penetration depth is no longer small compared to the body thickness and thus, the analytical solutions provided by all the above-mentioned studies are not valid. For typical engineering applications to laser cutting, or laser hardening of metals, the semi-infinite body assumption may not be a good one to make. Laser heating times, depending on the applications, can be of the order of millisecond to microsecond, or the equivalent of Fourier's number (i.e.,  $\tau$ , dimensionless time) of the order of  $10^6$  to  $10^7$  [1,19]. Jen and Gutierrez [8] present an analytical solution for the finite geometry with three different sets

of thermal boundary conditions, namely constant wall temperature, insulated and convection, at the “far” surface (i.e., surface far away from the laser heat input surface). They show that the size effect plays an important role in determining the temperature distribution, the maximum temperature and the location of the maximum temperature inside the workpiece.

Most of the early studies assume constant thermal properties throughout the domain. However, due to the high irradiation of the localized laser heat source, the thermal properties may change significantly due to the large temperature gradient near the laser heat source. Lesnic, et al. [10] solved the non-linear heat equation for temperature dependent thermal properties, employing the Kirchoff transformation. In their approach, a constant thermal diffusivity was assumed in order to linearize the heat equation. This provides a limiting case where the temperature variations in thermal conductivity and heat capacity are a similar function of temperature. To investigate the effects of temperature-dependent thermal properties for the general case, a numerical model has to be used. It should be noted that the analysis presented in this paper does not include radiation losses or phase change effects. If these effects are to be accounted for, additional mass and conservation equations have to be solved [18].

This paper presents a numerical study of the temperature distribution in a body subjected to a spatially exponential decaying laser source. The governing heat conduction equation, the boundary conditions and the initial condition are presented in a dimensionless form as a function of a group of dimensionless parameters, namely,  $\chi$ ,  $\tau$ ,  $Bi$ ,  $w$ ,  $c_1$ ,  $c_2$  and  $c_3$ . The governing

equation is discretized using a control volume approach with a variable grid to increase the resolution of the domain near the boundary where the laser heat source is applied. The influence of the different parameters and the temperature dependent thermal properties on the location and the magnitude of the maximum temperatures, as well as the local temperature distribution, are studied in detail. The calculated results are benchmarked against previous analytical studies for constant thermal properties obtained for both semi-infinite and finite domains. Finally, the present numerical solutions are compared to existing experimental data.

**2. Theoretical analysis**

Consider a laser heat source applied at the surface of a slab as shown in Fig. 1. The laser heat source is assumed to be decaying exponentially with time and depth into the slab material.

Allowing for temperature dependent thermal properties, the governing heat conduction equation with the laser heat source can be written as follows [1,20]

$$\rho C_p \frac{\partial T}{\partial t} = \frac{\partial}{\partial x} \left( k \frac{\partial T}{\partial x} \right) + q'''(x, t) \tag{1}$$

With reference to Fig. 1(a), the surface to which the laser heat source is applied (at  $x = 0$ ) is denoted as the “near” boundary. The other surface (at  $x = L$ ) is denoted as the “far” boundary. In this study, the insulated thermal boundary condition is imposed at the “far” boundary, and the convective thermal boundary condition imposed at the “near” boundary. The boundary conditions can be expressed as follows

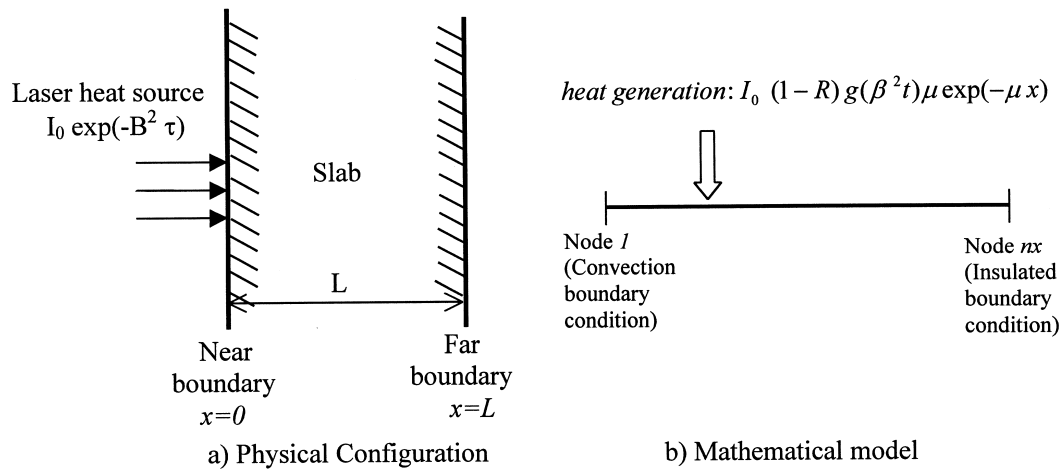


Fig. 1. Physical configuration and mathematical model.

$$\frac{\partial T}{\partial x}(0, t) + \frac{h}{k}(T_\infty - T(0, t)) = 0 \quad (2)$$

$$\frac{\partial T}{\partial x}(L, t) = 0 \quad (3)$$

The initial condition is assumed equal to the ambient temperature

$$T(x, 0) = T_0 \quad (4)$$

For a material that absorbs the laser energy internally, the heat generation term in Eq. (1) can be modeled as [20]

$$q''' = I_0(1 - R)g(\beta^2 t)\mu \exp(-\mu x) \quad (5)$$

where  $I_0$  is a reference laser incident irradiation,  $R$  is the surface reflectance,  $\mu$  is the absorption coefficient and  $g(\beta^2 t)$  is the time dependent laser input. This model assumes no spatial variation of the heat input in the plane normal to the laser beam and also assumes that heat diffusion perpendicular to the beam direction is negligible [1,20].

In most of the early studies, thermal properties were assumed to be constant. In reality, the large temperature gradient generated by this intensive laser heat source could result in significant thermal property variations. For most engineering materials, temperature-dependent thermal properties can be modeled as functions of temperature as follows [16]:

$$k = k_0 + k_1(T - T_0) \quad (6)$$

$$C_p = C_{p0} + k_2(T - T_0) + k_3(T - T_0)^2 \quad (7)$$

Now, if we define  $\theta(x, t)$  as the temperature rise above the initial temperature

$$\theta(x, t) = T(x, t) - T_0 \quad (8)$$

And the following dimensionless parameters are introduced

$$\xi = \mu x \quad \tau = \alpha \mu^2 t$$

$$Bi = \frac{h}{k_0 \mu} \quad B^2 = \frac{\beta^2}{\alpha \mu^2}$$

$$w = \frac{I_0(1 - R)}{h(T_\infty - T_0)} \quad u = \frac{\theta}{\frac{I_0(1 - R)}{k_0 \mu}} \quad (9)$$

$$c_1 = \frac{k_1 I_0(1 - R)}{k_0 \frac{I_0(1 - R)}{k_0 \mu}} \quad c_2 = \frac{k_2 I_0(1 - R)}{C_{p0} \frac{I_0(1 - R)}{k_0 \mu}}$$

$$c_3 = \frac{k_3}{C_{p0}} \left( \frac{I_0(1 - R)}{k_0 \mu} \right)^2$$

Substituting the above dimensionless parameters into the governing heat conduction equation, Eq. (1), a dimensionless equation is obtained:

$$\gamma \frac{\partial u}{\partial \tau} = \frac{\partial}{\partial \xi} \left[ \kappa \frac{\partial u}{\partial \xi} \right] + g(B^2 \tau) \exp(-\xi) \quad (10)$$

where  $\kappa = (1 + c_1 u)$  is the dimensionless thermal conductivity and  $\gamma = (1 + c_2 u + c_3 u^2)$  denotes the dimensionless heat capacity. Note that  $c_1$  is the dimensionless coefficients of the thermal conductivity equation and  $c_2$  and  $c_3$  are the dimensionless coefficients of the heat capacity equation (see Eqs. (6) and (7), respectively).

It has been demonstrated previously that maximum temperature gradients, due to the exponential decay in laser heat absorption into the workpiece, are in a very thin layer near the wall on the side where the laser is applied. For this reason, it is convenient to have very good grid resolution in this zone. In order to achieve this, a variable grid is used. An algebraic equation is used to transform the spatial coordinate  $\xi$  [5]

$$\xi = 0.1\chi + 0.90\chi^2 \quad (11)$$

where  $\chi$  is the transformed spatial coordinate. The modified Eq. (10)

$$\gamma \frac{\partial u}{\partial \tau} = \chi_\xi^2 \frac{\partial}{\partial \chi} \left[ \kappa \frac{\partial u}{\partial \chi} \right] - 0.18\chi_\xi^3 \kappa \frac{\partial u}{\partial \chi} + q^*(\chi, \tau) \quad (12)$$

Here  $\chi_\xi$  is the metric of the transformation given by

$$\chi_\xi = \frac{1}{0.1 + 0.18\chi} \quad (13)$$

and  $q^*(\chi, \tau) = g(B^2 \tau) \exp[-(0.1\chi + 0.90\chi^2)]$  is the dimensionless heat generation term.

The “near” thermal boundary condition (convection) can be written in dimensionless form as follows:

$$\chi_\xi \frac{\partial u}{\partial \chi}(0, \tau) - \frac{Bi}{(1 + c_1 u(0, \tau))} u(0, \tau) = -\frac{1}{(1 + c_1 u(0, \tau))w} \quad (14)$$

Similarly, the “far” thermal boundary condition can be written in dimensionless form as follows:

$$\frac{\partial u}{\partial \chi}(\chi^*, \tau) = 0 \quad (15)$$

The initial condition can be expressed in dimensionless form as:

$$u(\chi, 0) = 0 \tag{16}$$

It is worth noting that if constant thermal properties are assumed,  $c_1, c_2$  and  $c_3$  will be equal to zero. In this case, the governing equation becomes linear and analytical solutions can be obtained [8].

The solution of Eq. (10) can be expressed in the form

$$u = f(\chi, \tau, Bi, w, c_1, c_2, c_3, g(B^2\tau)) \tag{17}$$

Note that the parameter  $w$  only appears in the convection boundary condition. In general, this parameter is usually very large and its influence is negligible. It is important to point out that the solution is strongly dependent on the laser input profile. In the numerical model the laser input profile is easily specified through the heat source term in the governing equation (i.e., Eq. (12)). For a continuously operating laser source of constant strength,  $g(B^2\tau)$  is equal to one, and the functional form of the solution for a particular  $Bi$  becomes

$$u = f(\chi, \tau, c_1, c_2, c_3) \tag{18}$$

If our interest is in maximum or surface temperatures for a given Biot number and a specific laser input, the functional relation is not a function of  $\chi$  and can be written as:

$$u_{\max} = f(\tau, c_1, c_2, c_3)$$

or

$$u_{\text{surf}} = f(\tau, c_1, c_2, c_3) \tag{19}$$

Another case of interest is the relation between surface temperature as a function of the Biot number for the linear case ( $c_1, c_2$  and  $c_3$  are zero). In this case the functional relation can be written as

$$u_{\text{surf}}^* = f(\tau, Bi) \tag{20}$$

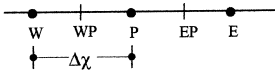
These cases will be studied in detail.

### 3. Numerical formulation for the non-linear case

In the numerical analysis presented below, a control-volume based method is used. As presented by Patankar [13], this method can be formulated to account for temperature-dependent thermal properties. The formulation is presented in a compact matrix form. In this formulation the implementation of the boundary condition as well as the method for time integration is performed very easily. In order to maintain second order accuracy in space, the central difference method is used for the diffusion term as follows:

$$\gamma_p \frac{\partial u}{\partial \tau} = \frac{\left(\chi_{\xi}^2 \kappa\right)_{EP} \frac{\partial u}{\partial \chi} \Big|_{EP} - \left(\chi_{\xi}^2 \kappa\right)_{WP} \frac{\partial u}{\partial \chi} \Big|_{WP}}{\Delta \chi} - 0.18 \chi_{\xi}^3 \kappa \frac{u_E - u_W}{2 \Delta \chi} + q_p^* \tag{21}$$

using central differences again for the spatial derivative



$$\gamma_p \frac{\partial u}{\partial \tau} = \frac{\left(\chi_{\xi}^2 \kappa\right)_{EP} (u_E - u_P) - \left(\chi_{\xi}^2 \kappa\right)_{WP} (u_P - u_W)}{\Delta \chi^2} - \frac{0.9 \chi_{\xi}^3 \kappa \Delta \chi (u_E - u_W)}{\Delta \chi^2} + q_p^* \tag{22}$$

grouping in the following way

$$\frac{\partial u}{\partial \tau} = \frac{\left(\chi_{\xi}^2 \kappa\right)_{EP}}{\gamma_p \Delta \chi^2} (1 - 0.9 \chi_{\xi} \kappa) u_E - \left( \frac{\left(\chi_{\xi}^2 \kappa\right)_{EP}}{\gamma_p \Delta \chi^2} + \frac{\left(\chi_{\xi}^2 \kappa\right)_{WP}}{\gamma_p \Delta \chi^2} \right) u_P + \frac{\left(\chi_{\xi}^2 \kappa\right)_{WP}}{\gamma_p \Delta \chi^2} (1 + 0.9 \chi_{\xi} \kappa) u_W + \frac{q_p^*}{\gamma_p} \tag{23}$$

naming the coefficients of the nodal temperatures as follow

$$K_E = \frac{\left(\chi_{\xi}^2 \kappa\right)_{EP}}{\gamma_p \Delta \chi^2} (1 - 0.9 \chi_{\xi} \kappa)$$

$$K_P = - \left( \frac{\left(\chi_{\xi}^2 \kappa\right)_{EP}}{\gamma_p \Delta \chi^2} + \frac{\left(\chi_{\xi}^2 \kappa\right)_{WP}}{\gamma_p \Delta \chi^2} \right)$$

$$K_W = \frac{\left(\chi_{\xi}^2 \kappa\right)_{WP}}{\gamma_p \Delta \chi^2} (1 + 0.9 \chi_{\xi} \kappa) \quad Q_P = \frac{q_p^*}{\gamma_p} \tag{24}$$

a matrix form is obtained

$$\frac{\partial u}{\partial \tau} = [K]\{u\} + \{Q\} \tag{25}$$

The more general difference scheme for time integration is given by the following expression:

$$u^{n+1} = u^n + (1 - \eta) u^n \Delta \tau + \eta u^{n+1} \Delta \tau \tag{26}$$

where  $\eta$  is a weighting factor, varying from zero to unity. The time derivatives may be eliminated by substituting  $\{u^n\} = [K]^n \{u^n\} + \{Q\}^n$  and similarly

$\{u^{n+1}\} = [K]^{n+1}\{u^{n+1}\} + \{Q\}^{n+1}$ . Now, plugging Eq. (26) into Eq. (25) and rearranging in a more convenient form yields

$$\begin{aligned} & (I - \eta[K]^{n+1} \Delta\tau) \{u^{n+1}\} \\ &= (I + (1 - \eta)[K]^n \Delta\tau) \{u^n\} + \Delta\tau \left( (1 - \eta) \right. \\ & \quad \left. \times \{Q\}^n + \eta \{Q\}^{n+1} \right) \end{aligned} \tag{27}$$

By writing

$$[A]^{n+1} = I - \eta[K]^{n+1} \Delta\tau \tag{28}$$

$$[B]^n = I + (1 - \eta)[K]^n \Delta\tau \tag{29}$$

and

$$\{Q\Delta\tau\}^{\binom{n+1}{n}} = (1 - \eta)\{Q\}^n \Delta\tau + \eta\{Q\}^{n+1} \Delta\tau \tag{30}$$

it is obtained

$$[A]^{n+1}\{u\}^{n+1} = [B]^n\{u\}^n + \{Q\Delta\tau\}^{\binom{n+1}{n}} \tag{31}$$

Note that  $u^n$  is known from previous computation (or from the initial condition if this is the first time step). Then, the product  $[B]^n\{u\}^n$  can be written as the vector

$$\{b\}^n = [B]^n\{u\}^n \tag{32}$$

The system of algebraic equations to be solved at each time step is

$$[A]^{n+1}\{u\}^{n+1} = \{b\}^n + \{Q\Delta\tau\}^{\binom{n+1}{n}} \tag{33}$$

It should be pointed out that the matrix  $[A]$  and the vector  $Q \Delta\tau$  are not constant as they are in the linear case. They are functions of the dimensionless thermal properties  $\kappa$  and  $\gamma$  at the current time step. Iterations are needed at each time step to update the matrix  $[A]$  and the vector  $Q \Delta\tau$  until convergence is reached. After this, we can proceed to the next time step and repeat the procedure.

For  $\eta = 0.5$ , the discretized equations are equivalent to the Crank–Nicholson scheme, and thus, second order accurate in both time and space and uncon-

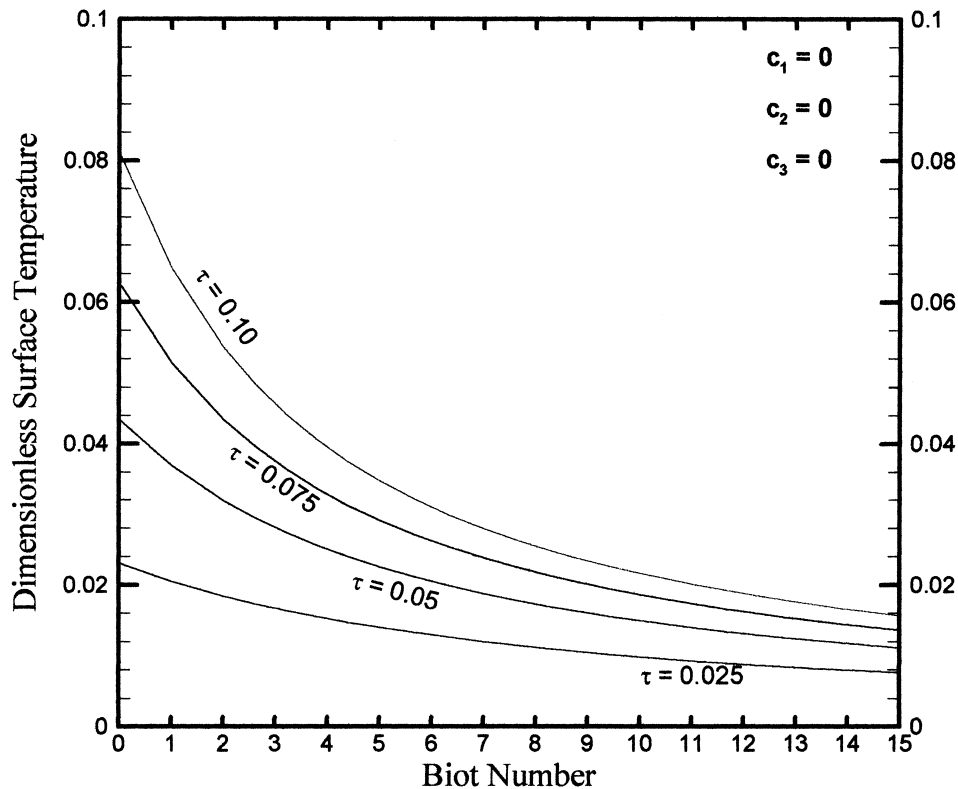


Fig. 2. Dimensionless surface temperature vs. Biot number.

Table 1  
Grid convergence test

$\chi$	$e_I = \frac{T_{II} - T_I}{T_{II}} \times 100$		$e_{II} = \frac{T_{III} - T_{II}}{T_{III}} \times 100$		$e_{III} = \frac{T_{IV} - T_{III}}{T_{IV}} \times 100$	
	$n_x = 100$	$\Delta t = 0.001$	$n_x = 200$	$\Delta t = 0.0005$	$n_x = 400$	$\Delta t = 0.00025$
0	0.41%		0		-0.15%	
0.4	0.52%		0		-0.27%	
0.8	0.45%		0		-0.23%	
1.2	0.31%		0		-0.12%	
1.6	0.27%		0		-0.10%	
2	0.15%		0		-0.08%	

ditionally stable. This scheme will be used throughout this study.

3.1. Implementation of convection boundary conditions

The convection boundary condition introduces new

terms in the coefficients  $A_{(1,1)}^{n+1}$ ,  $A_{(1,2)}^{n+1}$ ,  $B_{(1,1)}^{n+1}$ ,  $B_{(1,2)}^{n+1}$  previously calculated and an additional vector  $\{b_{inf}\}$  appears in the right-hand side of Eq. (33). This vector is zero everywhere except at node 1 where the convection boundary condition is defined. Using forward differences for the boundary condition at  $\chi = 0$  [12]

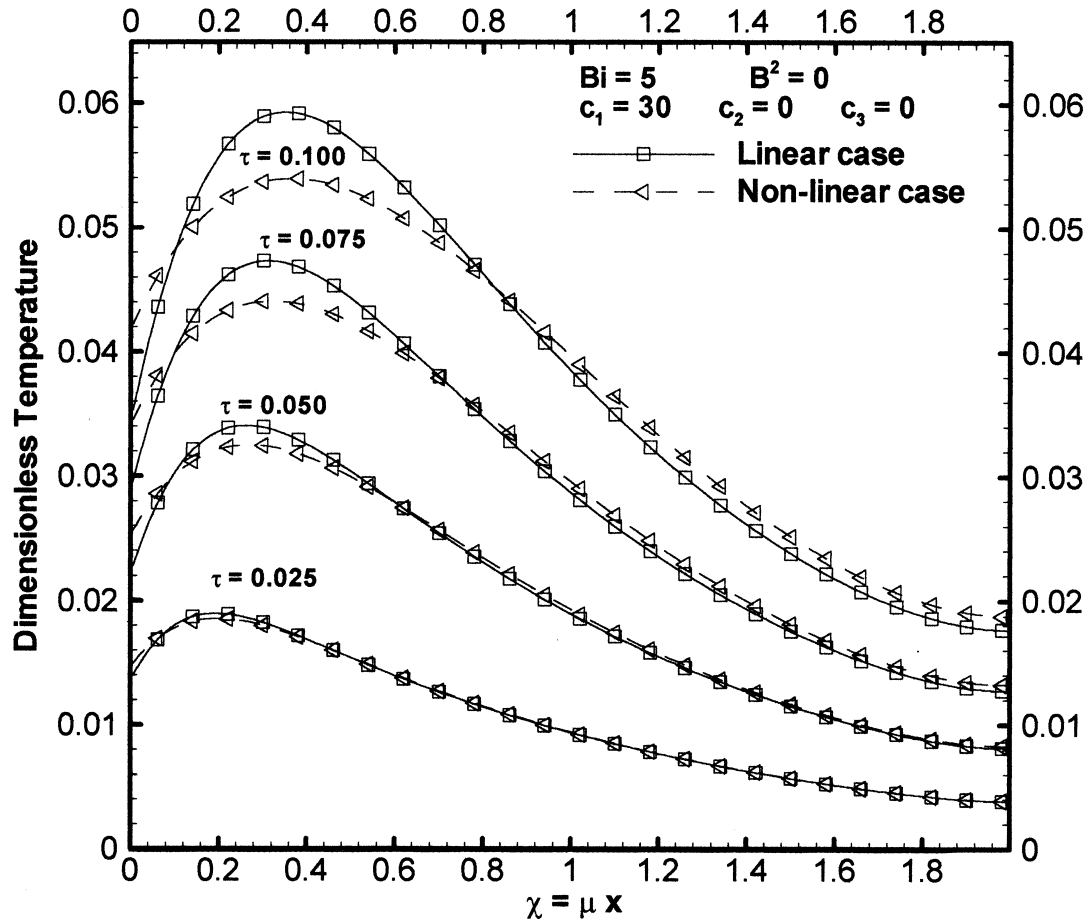


Fig. 3. Temperature profile for a positive dimensionless coefficient  $c_1$  associated with thermal conductivity.

$$A_{(1,1)}^{n+1} = A_{(1,1)}^{n+1} + \eta \frac{2\Delta\tau Bi \chi_\xi}{\Delta\chi \gamma_P^{n+1}} \quad (34)$$

$$A_{(1,2)}^{n+1} = 2A_{(1,2)}^{n+1} \quad (35)$$

$$B_{(1,1)}^n = B_{(1,1)}^n - (1-\eta) \frac{2\Delta\tau Bi \chi_\xi}{\Delta\chi \gamma_P^n} \quad (36)$$

$$B_{(1,2)}^{n+1} = 2B_{(1,2)}^{n+1} \quad (37)$$

$$b_{\text{inf}(1)}^{(n+1)} = \frac{2\Delta\tau(\kappa\chi_\xi)_1}{w\Delta\chi} \left( \frac{(1-\eta)}{\gamma_P^n} + \frac{\eta}{\gamma_P^{n+1}} \right) \quad (38)$$

3.2. Implementation of insulated boundary conditions

As a consequence of the insulated boundary condition at node  $nx$ , using backward differences at  $\chi = L$ , the coefficients  $A_{(nx,nx-1)}^{n+1}$  and  $B_{(nx,nx-1)}^n$  are changed to

$$A_{(nx,nx-1)}^{n+1} = 2A_{(nx,nx-1)}^{n+1}$$

$$B_{(nx,nx-1)}^n = 2B_{(nx,nx-1)}^n \quad (39)$$

Finally, in matrix form we obtain

$$[A]^{n+1} \{u\}^{n+1} = \{b\}^n + \{Q\Delta\tau\} \binom{n+1}{n} + b_{\text{inf}} \binom{n+1}{n} \quad (40)$$

where the coefficients of the vectors  $[A]^{(n+1)}$ ,  $\{b\}^{(n)}$ ,  $\{Q\Delta\tau\}^{(n+1)}$  and  $\{b_{\text{inf}}\}^{(n+1)}$  are as described previously.

3.3. Convergence test

The solution of the system given by Eq. (40) is obtained iteratively. Matrix  $[A]$  is evaluated based on the temperatures at the iteration  $n + 1$ . Since temperatures at the advanced iteration step are unknown, matrix  $[A]$  is initially computed based on the temperature at the current iteration. Eq. (40) can then be solved to obtain an updated value for temperature. This procedure is repeated until convergence. Differ-

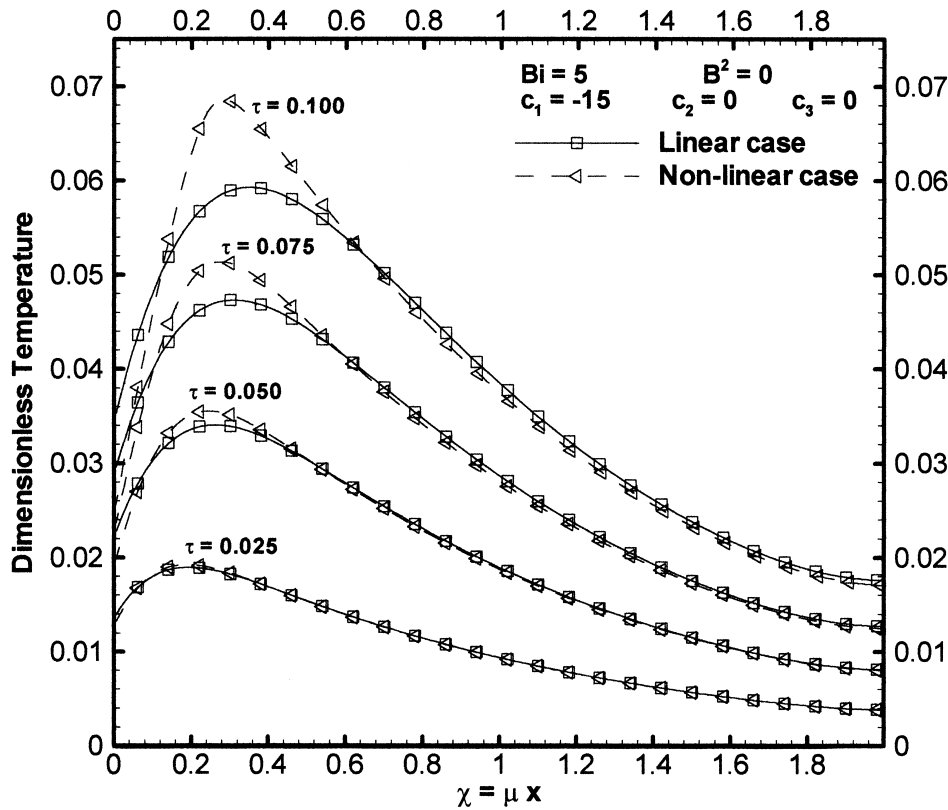


Fig. 4. Temperature distributions for constant laser heat source temperature profile for a negative dimensionless coefficient  $c_1$  associated with thermal conductivity.



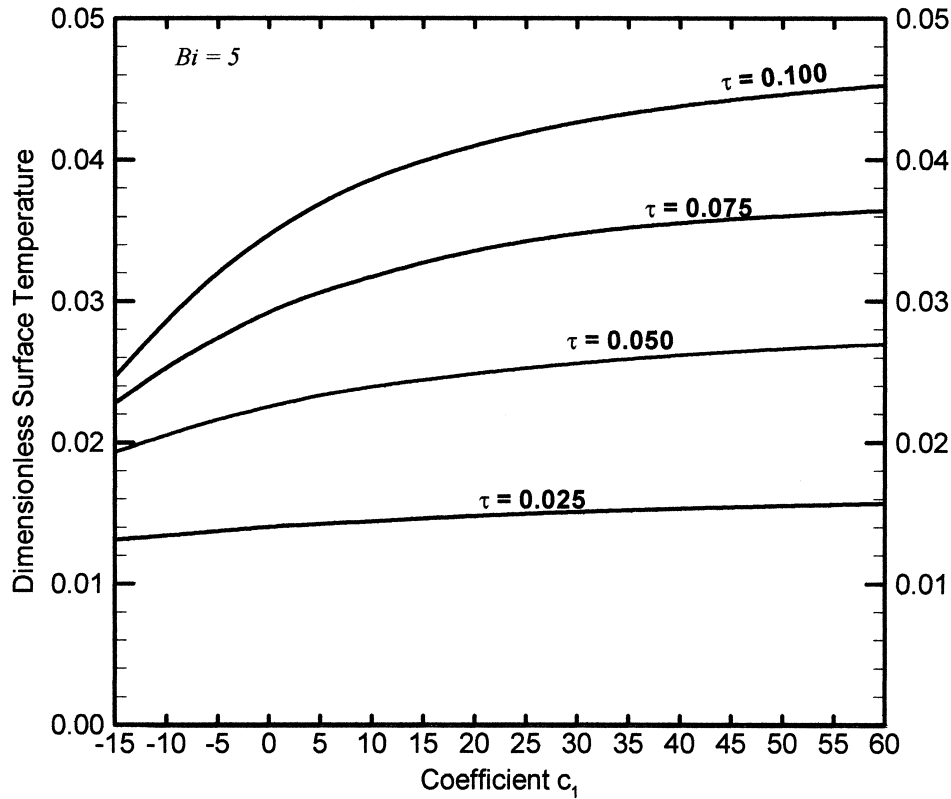


Fig. 5. Effect of coefficient  $c_1$  at the surface temperature.

ences in maximum temperatures were used to check this convergence. The error  $\varepsilon$  between two maximum temperatures corresponding to consecutive iterations  $n$  and  $n - 1$  are defined as:

$$\varepsilon = \frac{|T_{\max, n} - T_{\max, n-1}|}{T_{\max, n}} \times 100\%$$

This error must be less than the specified tolerance. In this study the tolerance was set equal to 1%. To test grid convergence, the time step  $\Delta\tau$  and the number of nodes in the space coordinate  $\chi$  was refined from (0.001, 100) to (0.00025, 400). It can be seen from Table 1 that the maximum error was less than 0.5%. This test was run for  $\tau = 0.1$  and Biot number equal to 5. From numerical experiments, the grid convergence is seen to be only weakly dependent on the Biot number and the value of  $\tau$  is the more exigent condition from the convergence point of view. Based on the grid convergence test, a time step size of 0.0005 and 200 nodes were used for the calculations presented in this work.

#### 4. Results and discussions

In the numerical study presented here, a constant heat source has been assumed ( $g(B^2\chi) = 1$ ). The primary interest in this work is in the effect of non-linearity due to temperature dependent thermal properties. Fig. 2 shows the relation between surface temperatures and Biot number for the linear case (i.e.,  $c_1, c_2$  and  $c_3$  are zero and  $\xi_{\max} = 1$ ) for different dimensionless times. It is seen from the figure that the effect of increasing Biot numbers above 10 give a small temperature reduction (less than 10%) at the surface. This is because the heat diffusion rate approaches a limiting value as the Biot number becomes larger at the “near” boundary. For Biot numbers of this order, a reduction of surface temperature by approximately 60% is seen for  $\tau = 0.1$  compared to the insulated surface condition case ( $Bi = 0$ ). In the following parametric studies, unless stated otherwise, a Biot number equal to 5 has been used. Increasing Biot number beyond a value of 5 results in a marginal reduction in maximum temperature. Physically, this means that the increased cost associated with increasing cooling at the boundary is not offset by a reduced maximum temperature.

In the sections that follow, the effect of non-linearity due to temperature dependent thermal property, as represented by the dimensionless coefficients  $c_1$ ,  $c_2$  and  $c_3$ , is analyzed in detail. Figs. 3 and 4 show the effect of the coefficient  $c_1$  (associated with thermal conductivity), for a Biot number equal to 5 and  $c_1 = 30$  and  $c_1 = -15$ , respectively. These values of  $c_1$  are representative typical engineering materials (noting that negative  $c_1$  values are valid only for limited ranges of temperature since thermal conductivity cannot become negative). In these figures, dashed lines with triangular symbols represent the case with variable thermal properties (non-linear case) and solid lines with square symbols denote the case of constant thermal properties (linear case). In Fig. 3, the parameters are  $c_1 = 30$ ,  $c_2 = 0$ , and  $c_3 = 0$ . Since  $c_1$  is greater than zero, the thermal conductivity increases as temperature increases. From the figure, it is observed that surface temperatures for the linear case are lower than for the non-linear case, although the maximum temperatures present in the slab are higher for the constant thermal property case. This can be explained as follows: when the laser heat source starts to act on the material, the heating process starts. A large temperature gradient is

generated in the vicinity of the “near” boundary. For the non-linear cases, this, in turn, increases the local thermal conductivity at the wall. Therefore, the thermal conduction resistance inside the solid slab becomes smaller, thus the convection resistance at the “near” boundary becomes larger. As one would expect, the surface temperature for the non-linear cases is thus larger than for the linear cases. It is instructive to point out the significant role of the non-linearity at the “near” boundary where a convection boundary condition is imposed. If we carefully examine this dimensionless “near” boundary condition, given by Eq. (14), a modified Biot number can be defined as follows:

$$Bi, m = \frac{Bi}{(1 + c_1 u^*)} \quad (41)$$

When the temperature increases, this modified Biot number,  $Bi, m$  decreases due to the positive value of the coefficient  $c_1$ . This implies that less heat is convected away from the “near” boundary (i.e., smaller Biot number). This explains why surface temperature for the non-linear cases is larger than the linear cases, even though the resulting thermal conductivity is

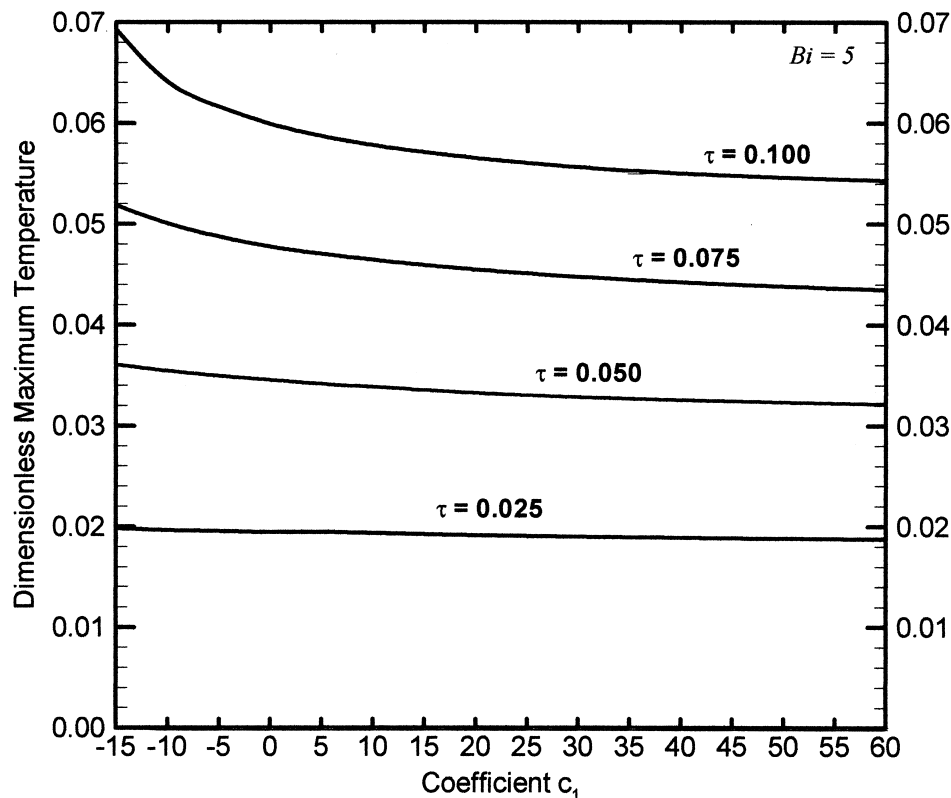


Fig. 6. Effect of coefficient  $c_1$  on the maximum temperature.

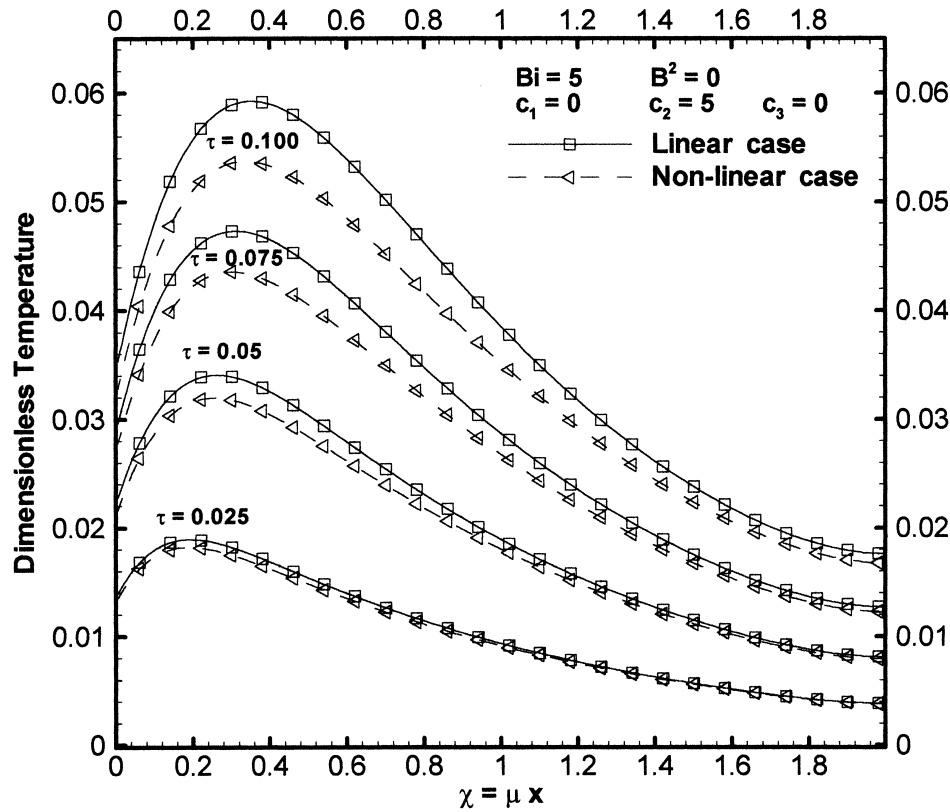


Fig. 7. Temperature profile for a positive dimensionless coefficient  $c_2$  associated with heat capacity.

higher for the nonlinear cases. For maximum temperatures, the lower temperatures for the nonlinear cases are simply because the thermal conductivity is greater for positive  $c_1$  values.

Fig. 4 shows the case for a negative  $c_1$ . In this figure, the parameters are  $c_1 = -15$ ,  $c_2 = 0$  and  $c_3 = 0$ . Since  $c_1$  is less than zero, thermal conductivity decreases as temperature increases. In comparison to the cases with positive  $c_1$ , the results are dramatically different. Since thermal conductivity decreases with temperature, maximum temperatures are higher for the non-linear cases, as seen in Fig. 4. However, surface temperatures are higher for the linear cases. These trends are opposite to that for the positive  $c_1$  case. This can be explained by revisiting Eq. (41). The modified Biot number,  $Bi$ ,  $m$ , increases as the surface temperature increases. This is due to the negative value of the coefficient  $c_1$ , as seen in the numerator of Eq. (41). It is observed from Fig. 4 that the surface temperature approaches a limiting value as time increases. This is because, for increasing time (increasing temperatures) the heat diffusion rate may reach its limiting value when the modified Biot numbers increase in value at the “near” boundary due to the negative value of  $c_1$ . Thus, maximum tem-

peratures have to increase because less heat can be removed from the “near” boundary and further heat penetration into the material is hindered by the lower thermal conductivity. In this case, the effect of variable thermal conductivity contributes to a more efficient explosive removal of material. Blackwell [1] gave an explanation for this phenomenon. He explained that as the material attains its maximum temperature, the phase change occurs inside the body instead of the exposed surface and the resulting material expansion produces the explosive removal.

Figs. 5 and 6 depict the effect of coefficient  $c_1$  on the surface and maximum temperatures respectively. The Biot number is 5. The  $c_1$  values were chosen to vary from  $-15$  to  $60$ , a very wide range representative of most of the typical engineering materials from plastics to metals. In Fig. 5, it is seen that for larger negative values of  $c_1$ , the surface temperature approaches a limiting temperature as time increases. For increasing positive values of  $c_1$ , the curves become flatter because the temperature gradients decrease and temperature profiles become more uniform. For a given time level, the surface temperature approaches a limiting value for increasing values of  $c_1$ . This is because as  $c_1$

increases, the modified Biot number approaches zero, i.e. the insulated boundary condition. Fig. 6 shows the maximum temperatures for various  $c_1$  values at different times. For fixed time, it can be seen that maximum temperature decreases for increasing  $c_1$ , to an asymptotic value. The behavior at large of  $c_1$  is a reflection of the fact that heat diffusion at the “near” boundary reaches its limiting value.

The non-linear effect of heat capacity on temperature distribution is shown in Fig. 7. In order to clearly demonstrate the effect of heat capacity, the value of  $c_1$  is set zero. The temperature-dependent heat capacity is represented by the coefficients  $c_2$  and  $c_3$ . In most of the parametric studies investigated (not shown), it is observed that the effect of  $c_3$  is relatively unimportant in comparison to  $c_2$ . Thus, in the presentation below, the discussion is concentrated on the effect of coefficient  $c_2$ . Dashed lines with triangular symbols represent the case with variable thermal properties and solid lines with square symbols denote the case with constant thermal properties. It is seen from the figure that, as one would expect, the temperatures for the variable heat capacity cases are smaller than for constant heat capacity cases. This is because the heat ca-

capacity increases for increasing temperatures ( $c_2$  is positive). More energy is required to raise the temperature of the body. If we examine the governing equation for this particular case (i.e.,  $k = \text{constant}$ ), by dividing the temperature dependent thermal capacity for both side, i.e.,

$$\frac{\partial T}{\partial t} = \frac{k}{\rho C_p} \frac{\partial^2 T}{\partial x^2} + \frac{q'''(x, t)}{\rho C_p} \quad (42)$$

We can see from this equation that the thermal diffusivity and the heat source intensity decreases as the temperature increases. Thus, this results in a decrease in temperature for variable thermal capacity cases

Figs. 8 and 9 depict the surface and maximum temperature as a function of  $c_2$  with  $c_1$  and  $c_3$  set equal to zero. In these cases, for increasing  $c_2$ , both surface and maximum temperature decreases. This can be explained again from Eq. (42) as mentioned above. It is worth noting that unlike the situation with  $c_1$ ,  $c_2$  does not play any role in the convection boundary condition.

A specific case study simulating an actual material has been performed and presented in Fig. 10. The ma-

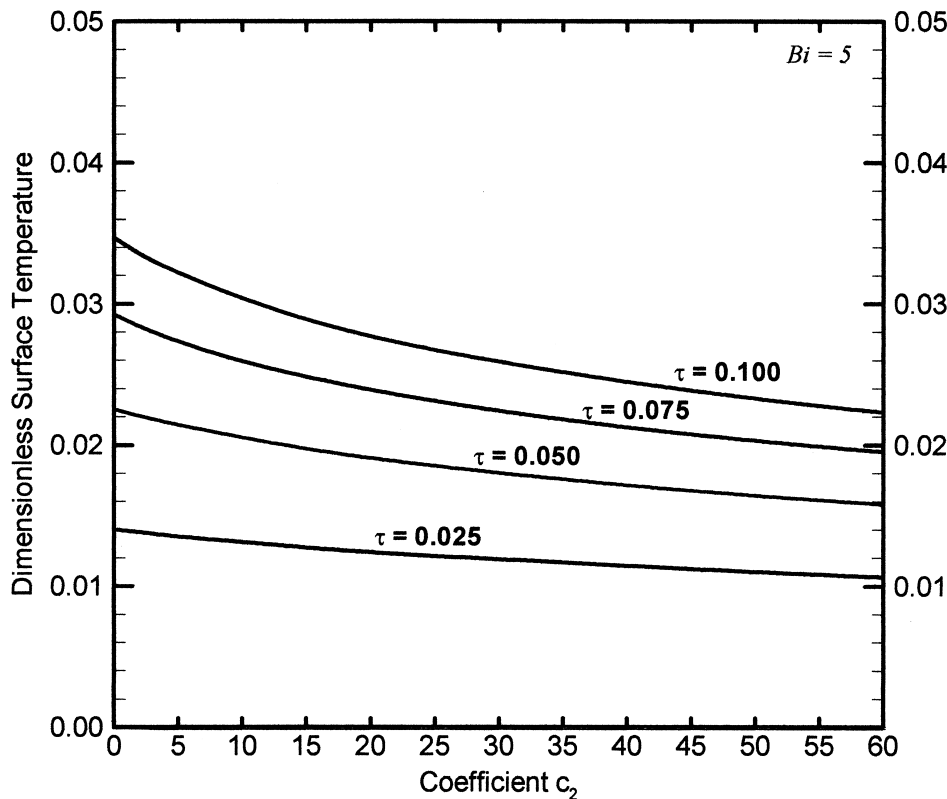


Fig. 8. Effect of coefficient  $c_2$  on the surface temperature.

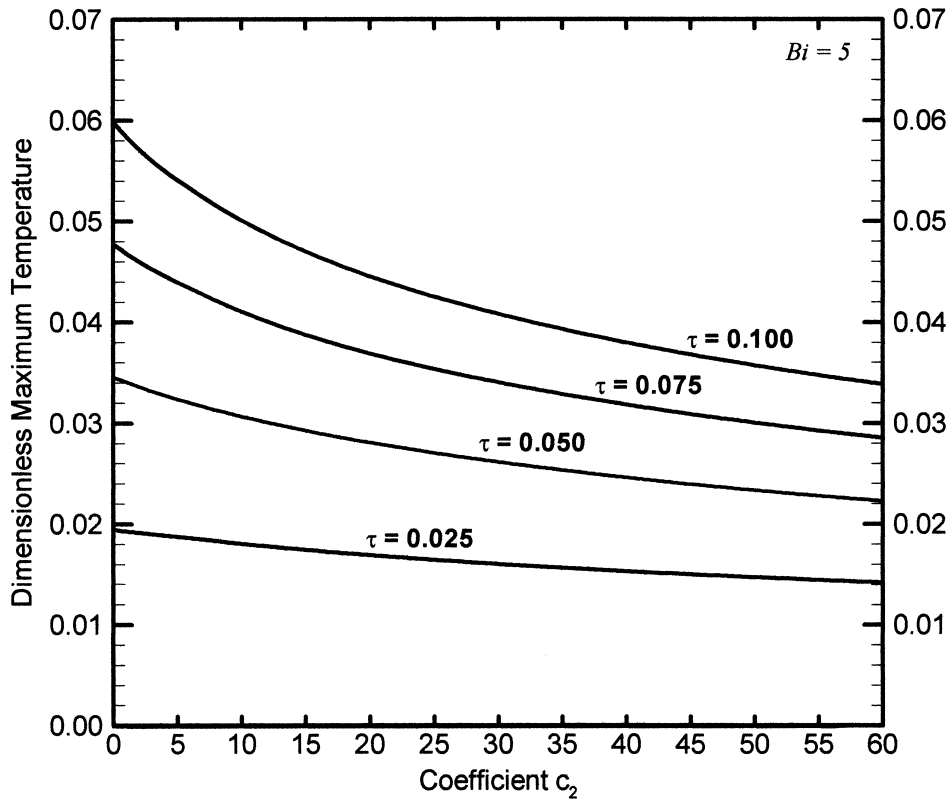


Fig. 9. Effect of coefficient  $c_2$  on the maximum temperature.

terial chosen is a sheet of polymethyl methacrylate (PMMA) of 1 mm thickness. The properties of the material are as follows:  $k_0 = 0.19$  W/(m K),  $\rho = 1180$  kg/m<sup>3</sup>,  $C_p = 1500$  J/(kg K),  $\mu = 5 \times 10^4$  m<sup>-1</sup>, softening temperature 400 K, and glass transition temperature 378 K. The time of application of the laser beam is  $10^{-3}$  s. The intensity of the source is  $I_0(1 - R) = 3 \times 10^7$  W/m<sup>2</sup>. Under this condition the maximum  $\xi$  is 50 ( $5 \times 10^4$  m<sup>-1</sup>  $\times 10^{-3}$  m). However, it is observed in numerical experimentation that for  $\xi > 5$ , the solution coincides with the analytical solution for the semi-infinite domain given by Blackwell [1], at least during the time of application of the laser beam. This means that, for a thickness of 1 mm, the far boundary condition is not felt at all and a value of  $\xi = 5$  can be used in the numerical computation. Values of  $k_1/k_0 = -10^{-3}$  K<sup>-1</sup>

and  $k_2/C_{p0} = 3 \times 10^{-3}$  K<sup>-1</sup> are assumed [3]. A heat transfer coefficient of 3000 W/(m<sup>2</sup> K) is used (note that a heat transfer coefficient of this magnitude can be obtained, for example, with an air gas jet velocity of 300 m/s). With these values, the calculated dimensionless parameters are  $\tau = 0.27$ ,  $Bi = 0.316$ ,  $c_1 = -3.16$  and  $c_2 = 9.48$ . From Fig. 10 it is seen that the maximum dimensionless temperature for the non-linear case is 0.125 (624 K, higher than the softening temperature) for  $\tau = 0.27$  and occurs at  $\xi = 0.15$ , that is, at 3  $\mu$ m from the wall. Due to the thermal expansion effect, an explosive removal of material could occur. From Fig. 10, it is seen that the effect of coefficient  $c_2$  is dominant and the non-linear model predicts lower temperatures even though the coefficient  $c_1$  is negative. In contrast to this, if a linear analysis is performed, the predicted

Table 2  
Thermal properties of the material used in the computation

Material	$k_0$ (W/(m K))	$k_1/k_0$ (K <sup>-1</sup> )	$C_{p0}$ (J/(kg K))	$k_2/C_{p0}$ (K <sup>-1</sup> )
PMMA	0.19	$-10^{-3}$	1500	$3 \times 10^{-3}$
Stainless steel	15.1	$9.7 \times 10^{-4}$	480	$3.75 \times 10^{-4}$

temperatures are usually higher and the explosive material removal will not necessarily occur.

To further verify the model predictions, the present numerical solution is compared with the existing experimental data from Yilbas [18]. In Yilbas' work, an Nd YAG laser with output energy of 15–30 J at 1.2–2.7 ms pulses was employed to irradiate a 1 mm thick stainless steel sheet. Stainless steel thermal properties used in the analysis are obtained from Incropera and Dewitt [7] (i.e.,  $k_0 = 15.1$  J/(m K),  $\rho = 8055$  kg m<sup>-3</sup>, and  $C_{p0} = 480$  J/(kg K)). The absorption constant,  $\mu$ , is chosen to be  $10^7$  m<sup>-1</sup> [1]. The reflectivity for the stainless steel changes from 0.1 to 0.3, thus an average value is used, i.e.,  $R = 0.80$  [11].

The temperature dependent thermal properties used in the computation of Figs. 10 and 11 are approximated using the following fitted equations:

$$k = k_0(1 + k_1/k_0\theta) \quad C_p = C_{p0}(1 + k_2/C_{p0}\theta)$$

where  $k_0$ ,  $k_1$ ,  $C_{p0}$  and  $k_2$  are given in Table 2.

Yilbas [18] measured the workpiece temperature using two photodetectors. The laser heating time is of the order of 50  $\mu$ s and the data were sampled at 5  $\mu$ s

intervals. Two data sets, corresponding to  $0.4 \times 10^{11}$  and  $0.6 \times 10^{11}$  W/m<sup>2</sup>, were presented from their experiment. These results are compared to the present numerical model as shown in Fig. 11. It can be seen that the agreement with the experimental data is reasonably good for the linear case except for the lower laser intensity input case (i.e.,  $I_0 = 0.4 \times 10^{11}$  W/m<sup>2</sup>). It is seen that better agreement is observed for the non-linear cases for both intensities except at smaller time. This may be due to the reason that at smaller time the parabolic heat conduction equation may not be valid, and a hyperbolic heat conduction (HHC) model may be more appropriate [4,6]. Furthermore, the effects of ablation of the material [18] and the experimental uncertainty may also contribute to the discrepancies.

## 5. Conclusions

A numerical study of temperature distribution subject to a laser heat source is presented. At the "near" boundary condition, a convection thermal boundary condition was imposed. A numerical code based on Crank–Nicholson scheme is developed to study the

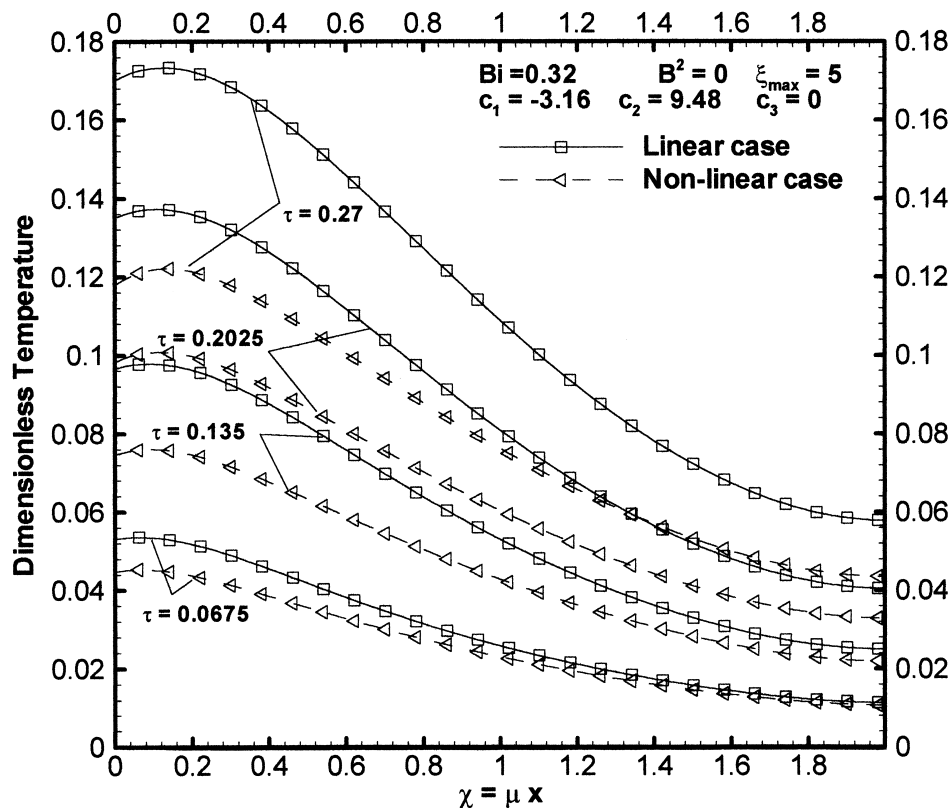


Fig. 10. Case study: sheet of polymethyl methacrylate (PMMA) of 1 mm.

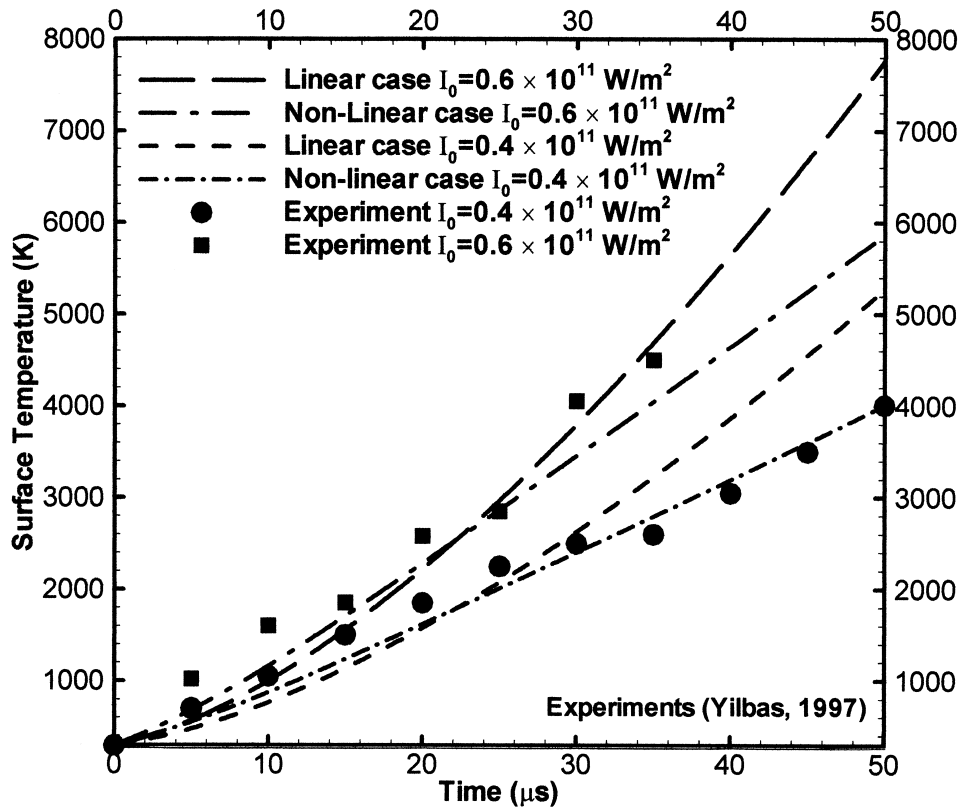


Fig. 11. Comparison to experimental data of Yilbas [18].

effects of temperature dependent thermal properties. The effects of non-linearity are studied through the dimensionless coefficients  $c_1$  associated with thermal conductivity and  $c_2$  and  $c_3$  associated with heat capacity of the materials. For positive  $c_1$ , the surface temperature increases and the maximum temperature decreases in comparison to the linear case. For negative  $c_1$  the effect is reversed. The effect of a positive  $c_2$  is to decrease temperatures because more energy is needed to increase the temperature of the body for increasing heat capacity coefficient. At high temperatures the effect of non-linearity is more apparent and cannot be neglected. The temperature profile can change its shape and magnitude depending on the relative importance of coefficient  $c_1$  (associated with thermal conductivity) and coefficient  $c_2$  and  $c_3$  (associated with heat capacity).

Comparison with experimental data shows better predictions for higher temperatures, as one would expect. The relatively good agreement between the model that has been developed and experimental data indicates that a one-dimensional conduction model can predict reasonably well the temperature distribution in the material.

#### Acknowledgements

Dr. Tien-Chien Jen and Mr. Gustavo Gutierrez would like to thank General Motors, UW System Applied Research Award and Society and Manufacturing Engineers (Research Initiation Award) for their financial support to the project. Dr. Stanley Chen's assistance in proofreading and in discussions is also acknowledged.

#### References

- [1] B.F. Blackwell, Temperature profile in semi-infinite body with exponential source and convective boundary condition, *ASME J. Heat Transfer* 112 (1990) 567–571.
- [2] F.W. Dabby, U. Paek, High-intensity laser-induced vaporization and explosion of solid materials, *IEEE J. Quantum Electron* QE-8(2) (1972) 106–111.
- [3] H.G. Elias, *An Introduction to Plastics*, VCH, New York, 1993.
- [4] Glass et al., Hyperbolic Stefan problem with applied surface heat flux and temperature-dependent thermal conductivity, *Numer. Heat Transfer A18* (1990) 503–516.

- [5] J.D. Hoffman, *Numerical Methods for Engineers and Scientists*, McGraw-Hill, New York, 1992.
- [6] M. Human, Non-Fourier heat transfer in laser heated metal surfaces, in: J.H. Kim, et al. (Eds.), *Heat Transfer — Korea–USA Seminar*, 1986, pp. 521–533.
- [7] F.P. Incropera, D.P. Dewitt, *Fundamentals of Heat and Mass Transfer*, Wiley, New York, 1996.
- [8] T.C. Jen, G. Gutierrez, Heat conduction in a finite region due to a time dependent laser source, in: *Proceedings of the 1999 National Heat Transfer Conference*, Albuquerque, New Mexico, August 15–17, 1999 (also published in the CDROM NHTC 99-142).
- [9] W. König, A. Wageman, *Laser assisted hot machining of ceramics and composite materials*, National Institute of Science and Technology, 1991. NIST Special Publication 847.
- [10] D. Lesnic, L. Elliot, D.B. Ingham, A note on the determination of the thermal properties of a material in a transient nonlinear heat conduction problem, *Int. Comm. Heat Mass Transfer* 22 (4) (1995) 475–482.
- [11] M.F. Modest, *Radiative Heat Transfer*, McGraw-Hill, New York, 1993.
- [12] M.N. Özisik, *Boundary Value Problems of Heat Conduction*, International Textbook Company, Pennsylvania, 1968.
- [13] S.V. Patankar, *Numerical Heat Transfer and Fluid Flow*, Hemisphere, New York, 1980.
- [14] J.C. Rozzi, F.E. Pfefferkorn, F.P. Incropera, Y.C. Shin, Transient thermal response of a rotating cylindrical silicon nitride workpiece subjected to a translating laser heat source. Part I: comparison of surface temperature measurements with theoretical results, *ASME J. Heat Transfer* 120 (1998) 899–906.
- [15] J.C. Rozzi, F.P. Incropera, Y.C. Shin, Transient thermal response of a rotating cylindrical silicon nitride workpiece subjected to a translating laser heat source. Part II: parametric effects and assessment of a simplified model, *ASME J. Heat Transfer* 120 (1998) 899–906.
- [16] D.A. Stephenson, J.S. Agapiou, *Metal Cutting Theory and Practice*, Marcel Dekker, New York, 1996.
- [17] K. Uehara, H. Takeshita, Cutting ceramics with a technique of hot machining, *Annals of the CIRP* 35 (1986) 55–58.
- [18] B.S. Yilbas, Laser heating process and experimental validation, *Int. Comm. Heat Mass Transfer* 40 (5) (1997) 1131–1143.
- [19] B.S. Yilbas, M. Sami, Convergence of time exponential decaying pulse to intensity input pulse for laser heating of semi-infinite body, *Int. Comm. Heat Mass Transfer* 24 (6) (1997) 785–791.
- [20] S.M. Zubair, M.A. Chaudhry, Heat conduction in a semi-infinite solid due to time dependent laser source, *Int. J. Heat Mass Transfer* 39 (14) (1996) 3067–3074.